COMPDYN 2011
3rd ECCOMAS Thematic Conference on
Computational Methods in Structural Dynamics and Earthquake Engineering
M. Papadrakakis, M. Fragiadakis, V. Plevris (eds.)
Corfu, Greece, 25–28 May 2011

PERFORMANCE INDICATOR OF A BRIDGE EXPANSION JOINT

Ivo M. Kalkman[1], Sven S.K. Lentzen[1], Wim M.G. Courage[1], Oswaldo Morales Napoles[1], and Flavio M.B. Galanti[1]

[1] TNO Built Environment and Geosciences
Van Mourik Broekmanweg 6, 2628 XE Delft, the Netherlands
e-mail: (ivo.kalkman, sven.lentzen, wim.courage, oswaldo.moralesnapoles, flavio.galanti)@tno.nl

Keywords: Structural Health Monitoring, Expansion Joint, Inverse Modeling, Failure Parameters, Damage Prediction, Maintenance Planning.

Abstract. *In general the condition of a structure can be assessed in terms of a performance indicator. For example, this can be the strength of a structure. An asset manager is concerned with ensuring that the performance of a structure does not fall below a given minimum level. This can be achieved by inspecting or monitoring the structure. As the performance indicator decreases with time, the asset manager can decide to take pre-emptive measures to restore the condition to its initial level, thus avoiding getting too close to the minimum required level. In order to work this way, it is important to define a reliable performance indicator. Following an inventory of structures which are prone to some form of degradation over time, a modular bridge expansion joint was selected as a case to be considered in this investigation.*

In order to determine the observability of known failure mechanisms in terms of modal and spectral data an experiment is set up which can simulate the construction under these circumstances. Further, a Finite Element Model of the construction is made, which is tuned to the experimental setup. This model is used to validate the applied inverse modeling technique to identify the failure parameters. The inverse modeling is performed using a genetic algorithm.

Through inverse modeling of the monitor data, changes over time of the identified failure parameters are obtained. In order to predict the development of the observed failure parameters in the future, these changes over time are incorporated in a prediction model. Taking uncertainties into account, stochastic processes are used to describe the degradation process. Thus, different types of processes can be used, e.g. Markov chains for discrete state changes in time or Gamma processes for continuous quantities in time. By continuously updating the prediction model with the monitor data, a risk based maintenance management tool is obtained by which pro-active and well-planned maintenance actions can be decided on. The developed methodology is applied to a full scale monitoring system of a real bridge in the Netherlands.

1 INTRODUCTION

Bridge expansion joints generally require a lot of maintenance. Replacing an expansion joint usually requires closing off (part of) the bridge which, together with the cost of the joint itself, makes this type of maintenance very expensive and a possible cause of major traffic disruptions. In order to determine the best moment to perform maintenance it is advantageous to be able to continuously monitor the state of the expansion joint. At the moment the condition of joints is normally checked by carrying out visual inspections at regular intervals. These visual inspections rely heavily on the experience and judgement of the inspector while some types of damage may not be visible at all. This introduces a relatively large uncertainty which, given the cost of replacement of the expansion joint, is highly undesirable. If the remaining serviceable lifetime can be estimated in a non-invasive manner with greater certainty the cost savings involved could therefore be substantial.

In this paper the non-invasive detection of damages to a modular bridge expansion joint by ambient vibration monitoring will be discussed as a possible alternative to visual inspection. The theoretical background behind this technique is presented in section 2. The current investigation consists of four distinct parts: lab tests on part of a joint, damage detection by inverse modeling, extrapolation of detected damages using a degradation model and extraction of guidelines for ambient vibration measurements. These are subsequently discussed in sections 3 through 6. In section 7 the ongoing effort of validation of these techniques using a real bridge are briefly discussed. A summary and conclusions are given in section 8.

2 THEORY

2.1 Damage detection

From experience it is known that structural damage can manifest itself through changes in natural frequencies, modal shapes and damping factors [1]. Changes in the frequencies and modal shapes of lower eigenmodes are generally an indication of global damage whereas changes at higher eigenmodes are often indicative of local damage. In the case of localized damage the amount of change in modal shape is usually highly frequency dependent and especially pronounced near the damaged part of the structure and behind it (as observed from the direction of the excitation source).

When trying to solve the inverse problem of determining damage parameters from a measured dynamic system response several practical problems are encountered [2]. One of these is the relatively limited amount of sensors in any practical measurement setup, as a result of which the observation of local changes in mode shapes due to local damage becomes a matter of chance. This might be mediated somewhat by the placement of sensors in positions where damage is most likely (i.e. near welds or areas of high stress) but it doesn't solve the problem completely.

More serious are the problems related to ill-conditioning, such as the question of uniqueness: it is conceivable that different types of damage have very similar effects on the observables monitored in the experiment, in which case the type of damage that has occurred can only be extracted from the measurement data with great difficulty, if at all. Among the possible solutions to this problem are the judgemental placement of sensors (ideally based on model calculations done before the actual measurements), the use of high precision sensors, placing a large number of sensors and measuring over long periods of time.

In addition to all of the above the number of parameters that can be varied in a typical (FEM) model of even a single joint is very large. This means that it is impossible to try and fit all of them to the measurement data. Therefore a small number of possible damages has to be

selected and only the parameters involved in those damage mechanisms are used as model input. However, it is obvious that any damage mechanism not considered beforehand will thus be overlooked. For these types of damage the model will therefore only be able to detect that a change has occurred, without being able to specify its cause.

2.2 Ambient vibration monitoring

In lab tests both the static and the dynamic response of the joint to a known excitation are measured (see section 3). However, for the purpose of monitoring real-life systems the use of artificial excitation sources has several drawbacks, for instance:

- The size of real-life systems is usually large, which means powerful excitation devices are needed. These devices are expensive and cumbersome, requiring a lot of time for their installation. Furthermore, in certain situations their size may be prohibitive
- The excitation of the structure due to traffic is generally much stronger than that due to (powerful) artificial excitation devices. Therefore, in order to perform sufficiently sensitive measurements, the bridge normally has to be closed off

As a result it has become common practice to monitor the dynamic response of a structure to ambient excitations (i.e. road traffic, wind, earthquakes etc.) instead. In the analysis these ambient forces are usually modeled as white noise. Although this assumption may introduce a modeling error and, given the statistical nature of the ambient forces, measurements have to be taken over a sufficiently large period of time, these shortcomings are normally outweighed by the advantages over artificial excitation.

2.3 Evolutionary algorithms

The solution process for any inverse problem is inherently iterative in nature. Many different algorithms have been developed for this purpose. Inverse modeling of damages is a global optimization problem where many local minima in solution space might exist. A global optimizer therefore has to be chosen, such as Monte Carlo methods, swarm-based optimization algorithms or neural networks. For the current investigation genetic algorithms were chosen, which belong to the more general class of evolutionary algorithms.

While many different implementations of evolutionary algorithms exist they are all based on the same general principles, inspired by the processes of reproduction and natural selection in nature. The concepts common to these implementations will briefly be discussed.

An individual is a trial solution to the problem and therefore consists of a complete set of parameter values that is necessary for the description of such a solution. In a first step the value of every parameter is chosen at random, each within a range set by the user. A given number of individuals (called a population) is generated this way, after which the quality of each individual is evaluated. This evaluation proceeds through a fitness function which quantifies the agreement between the trial solution and the target solution. The general idea is now to use the information contained in the best solution(s) (called parent(s)) in the generation of a new set of trial solutions (offspring). The creation of new trial solutions in each generation based on the best solution(s) from last generation ensures that the best solution will progressively improve. This process continues cyclically until the fit has converged.

The most popular evolutionary algorithm is probably the genetic algorithm. In this method the parameter values from two parents are randomly combined to create the offspring. To protect the algorithm from getting stuck in a local minimum of the error landscape some parameter values are changed at random for a small number of solutions, called a mutation. To make

sure that the best solutions do not deteriorate between generations they are allowed to survive unaltered from one generation to the next (elitism). The solution process is depicted in figure 1.

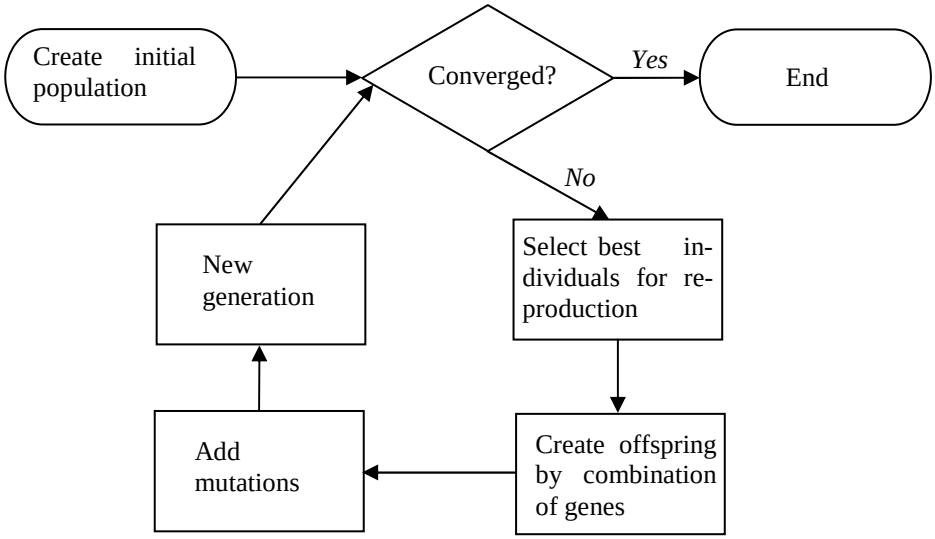

Figure 1: Genetic algorithm flowchart

As can be concluded from the above the genetic algorithm is basically stochastic in nature. This means that, depending on the complexity of the parameter space under investigation, convergence will be harder to achieve with increasing size of the parameter space. Although this effect can be countered by increasing the population size this will also increase the computational cost. For this reason it is very important to restrict parameter space as much as possible before a calculation is started. Unless the fitness function values for different possible solutions are suspected to be very close to each other it is therefore good practice to only include the parameters the final solution is most sensitive to in an initial fit and include the remaining parameters in a second, independent fit where the parameter range for the first set of parameters is much reduced.

3 LAB TESTS

3.1 Test setup

The full-size expansion joint mimicked in the lab tests is depicted in Figure 2. It is comprised of an edge beam, three center beams and a second edge beam arranged in the longitudinal direction of the joint with interposed elastomeric strip seals. The center beams are supported on cross bars (support bars) which bridge the structural gap. Each center beam has an individual set of support bars ensuring an independent movement of the center beams relative to each other. Support bars are placed at about 2m intervals and are grouped in sets of three. Each such set of support bars is inserted within a metal box which is fixed to the main structure. Each support bar rests on two sliding bearings.

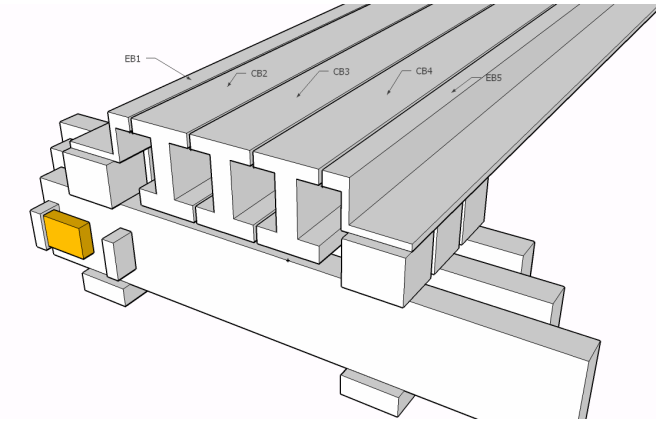

Figure 2: An example of a modular bridge expansion joint

The type of joint investigated can be prone to a number of different damage mechanisms as observed in the past:

- Wear and tear of sliding supports
- Wear and tear of control springs
- Failure of center beams or support bars
- Failure of weld joints between support bar and center beam
- Misalignment or breaking off of sliding supports
- Defects in strip seals

The experimental model consists of one single center beam on 5 support bars. The selected center beam is the first of the three center beams and is therefore located asymmetrically with respect to the support bar. The center beam is modelled using a HEM100 profile which has similar section properties as the beam used in the real expansion joint. The support bars on the other hand have identical dimensions as the real ones. The same sliding supports (sliding bearing and sliding spring) are used as in the real joint. The whole structure rests on two concrete plates placed in a bed of mortar of about 2 cm thickness on top of the laboratory floor. The sliding bearings and sliding springs are kept in place by a top steel plate which is fixed to the concrete plate via two threaded rods. The sliding bearing and spring can be positioned in such a way to simulate a closed joint as well as an open joint. Details of the lab model of the joint can be seen in Figures 3 and 4. The configuration depicted is that of a closed joint.

Figures 3 and 4 show side and top views of the lab model, respectively. The lab model has a total length of 7.5m, with support bars at intervals of approximately 1.8m. For reference purposes, a grid is defined consisting of 5 vertical lines numbered 1 to 5 and two horizontal lines indicated by ‘a’ and ‘b’. The 5 vertical lines correspond to the positions of the support bars. Lines ‘a’ and ‘b’ correspond to the long and short ends of the support bar, respectively. A Cartesian coordinate system is chosen such that the *x*-axis is parallel to the center beam, the *y*-axis is perpendicular to the center beam and the *z*-axis points upwards.

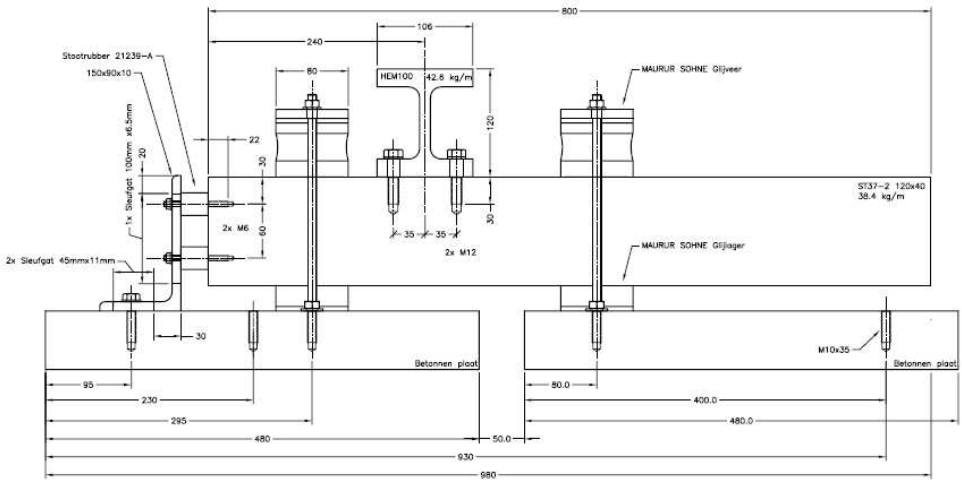

Figure 3: Side view of the lab model

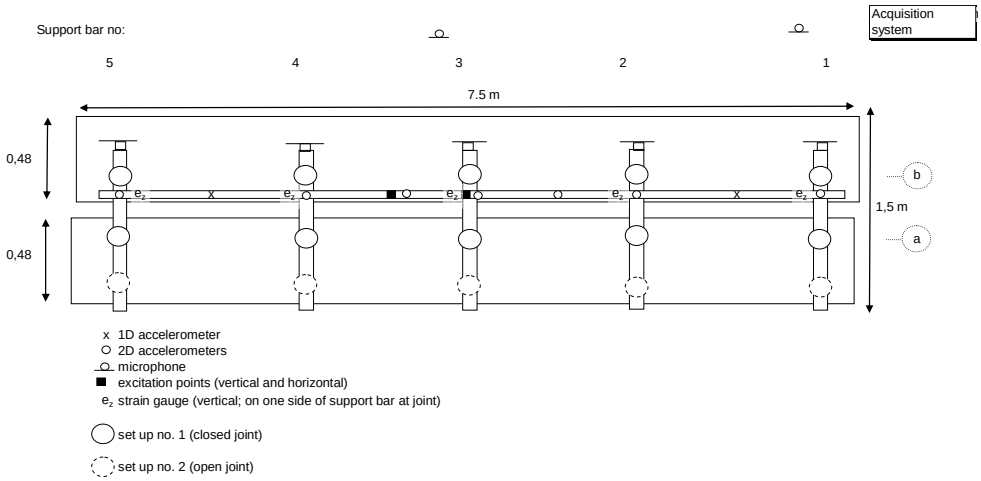

Figure 4: Top view of the lab model (schematic)

In the lab tests the objective is the reverse of that in the subsequent parts of the project: to investigate the effect of damage to the joint on measurable parameters in order to determine which quantities should be monitored. Several different observables were therefore monitored in the lab tests: accelerations of the center beam parallel and perpendicular to the road surface, strains and deflections of the support bars in the vertical direction (w.r.t. the road surface) and sound at some distance from the joint. An extensive set of measurements of both the static and dynamic response of the lab joint was carried out using accelerometers, strain gauges, microphones and laser triangulation sensors. The lab model allowed mimicking of all known damages mentioned in the previous section apart from the first (wear and tear of sliding supports) and the last (defects in strip seals).

3.2 Results

For lack of space only a small part of the tests which were performed are presented here. A single dynamic excitation of a 1000 kg weight impacting the center beam in vertical (negative *z*) direction between support bars 3 and 4 was therefore selected. Some of the recorded responses will be presented in section 4: here only the conclusions are discussed.

Control spring failure was not detected with the chosen observation quantities. This holds for any excitation position and any excitation direction.

A half saw cut in the support bar can be detected, though the effects are not significant. The main change is increased damping in the damaged support.

A half saw cut in the center beam can be detected with the investigated observation parameters. Compared to the effects of a half saw cut in one of the support bars the effects of a cut in the center beam are similar but more pronounced.

Loose joints can only be detected with the chosen observation parameters when the central beam is excited in *y*-direction and the dynamic parameters are determined in the same direction. In this case the main changes are larger displacements above the supports and different bending moments in the support bars. For the excitation considered in this paper, which is in the *z*-direction, no significant change is observed.

The failure of a support is very easily detectable: in the case of a single support this leads to the occurrence of a low frequency mode at about 25 Hz. At this mode the support bar vibrates at high amplitudes and low damping.

The effects of combined failures can roughly be superimposed.

4 INVERSE MODELING

4.1 Model definition

A finite element model of the bridge joint was constructed in Matlab. The model is very flexible, allowing the number of structural members (beams and support bars), the joint geometry and all material parameter values each to be set by a single variable. For a given set of parameter values it will then calculate eigenfrequencies, eigenmodes and the system response to a given input. This setup was chosen because it gives optimization routines written in Matlab direct access to all relevant parameters. An example of a bridge joint created with this Matlab script is given in Figure 5. In the following all relevant components of the model will be discussed in more detail.

First the number of beams and support bars, their sizes and their positions relative to each other and to the joint supports need to be specified. The number of elements to be used for each joint section is also selected. Based on this geometric information the script will construct a global coordinate system as well as local coordinate systems for both the beams and support bars; however, in this paper the global axis system indicated in Figure 4 will be referred to exclusively. It will then derive the coordinates of each element. In addition, in order to be able to fully specify how beams and support bars are connected, a small connection element which also carries its own local axis system is introduced between beams and support bars.

After this is done the material parameters for the beams, support bars and connection elements need to be specified: Young's Modulus (*E*), shear modulus (*G*), mass per unit length (*Mu*) and torsional mass per unit length (*J*). The connections between support bars and joint supports, which are made of rubber, are modeled as a spring-damper system in all 6 degrees of freedom (translations and rotations around all three local axes), corresponding with a total of 12 degrees of freedom (i.e. 6 for the springs and 6 for the dampers).

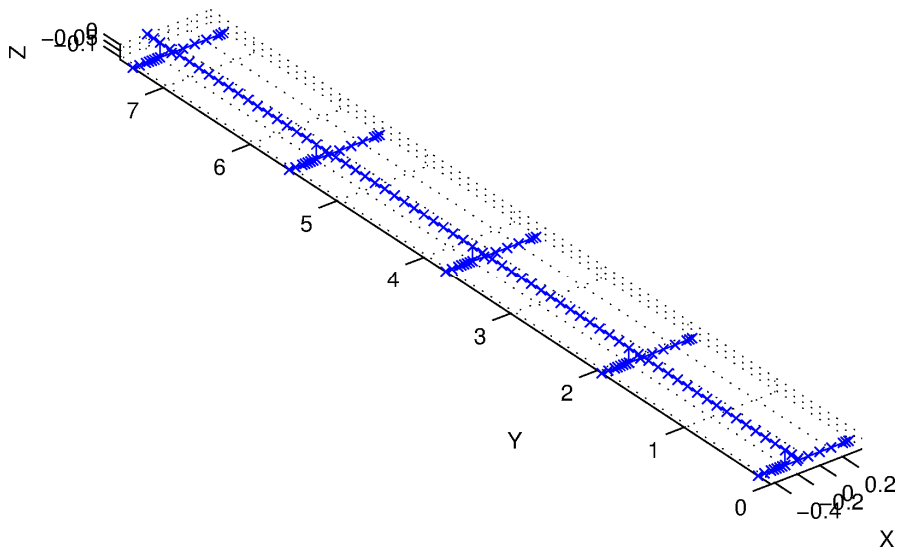

Figure 5: An example of a bridge joint model with a single beam and five support bars generated with the joint Matlab script. Each cross indicates a node of the FEM model. Also indicated is the axis system.

Each section of the joint is modeled as a Timoshenko beam with independent bending along the local y- and z-axes and torsion along the local x-axis. To this end the script has to be provided with five additional geometric parameters each for the beams, support bars and connections: cross sectional area, shear cross sectional area, bending inertia about the local y- and z-axes and torsional inertia about the local x-axis.

After the model has been defined the system matrices are set up and the eigenmodes and eigenfrequencies are calculated. When a time-dependent force acting on the system is now defined the response in each mode can be derived using the Newmark routine, after which all modal responses are added to yield the total system response. In this process a modal damping factor can be specified for each individual mode. Since the number of modes involved is usually so large that it is impractical to actually do so, in practice the damping values are obtained by interpolation from a table containing damping factors at a number of fixed frequencies.

4.2 Model tuning

Before a start can be made with the modeling of damages, the parameter values which are not precisely known from the experiment have to be fit by comparison of measured and calculated system responses for the undamaged joint. This process, termed model tuning, will be discussed in the following.

The model presented here contains 22 parameters for which their values were deemed to be uncertain enough to be included in the tuning process: the cross sectional area, shear cross sectional area, bending inertia about the x- and y-axes and torsional inertia about the z-axis for the connection element between beam and support bars; the six spring stiffnesses for the connection between support bars and joint supports; and eleven modal damping values at various frequencies.

For the tuning of the model a single measurement from the experiment was chosen, namely a dynamic excitation in z-direction (vertical), in the middle between support bars 3 and 4 (hereafter denoted as position 3.5). Even though the time trace of the corresponding excitation force is available from the measurements, in environmental vibration monitoring this excitation force is often unknown and therefore modeled as white noise (see section 2.2). For this reason the excitation force time trace was used as input for the Matlab model, in order to en-

able a comparison with the lab data which is as good as possible, but not in the comparison itself. Instead, the mobilities at different positions on the beam were chosen as the monitoring variables, as these contain information about the system as a whole yet are independent of the excitation force. Since the mobility becomes singular for zero force only those mobilities were used in the fitting procedure for which the corresponding force was at least 1% of its maximum value. As a result the mobility spectra throughout this paper feature gaps at those frequencies where this condition doesn't hold.

The parameter optimization problem at hand is clearly complex: it contains many variables (22) and the parameter ranges for most of these variables are very large, spanning several orders of magnitude. Such a parameter space can be very wild and erratic containing many local minima. In order to ensure the stability of the optimization process a global optimizatizer should therefore be used. For the present investigation a genetic algorithm (see section 2.3) was considered most appropriate and was therefore used throughout. As a fitness function the weighted normalized difference between measured and calculated mobilities was chosen:

$$fitness = \sum_i w_i \, || \, mob_c^{\,i} - mob_m^{\,i} \, || \, / \, || \, mob_m^{\,i} \, ||, \tag{1}$$

where mob_c and mob_m indicate the calculated and measured mobility, respectively, and the sum runs over all measurement positions that are included in the evaluation. The relative weights w_i of the measured spectra are chosen to be proportional to the maximum mobility values in these spectra with $\sum w_i = 1$. From this definition it can be deduced that for trial solutions of comparable norm as the measured mobility ($|| \, mob_c^{\,i} \, || \approx || \, mob_m^{\,i} \, || \, \forall \, i$) the given fitness function is approximately normalized, with a value ~1 meaning no correspondence whatsoever and 0 indicating perfect agreement. Correspondingly, it can be viewed as a measure of discrepancy between calculated and measured spectra, with for example a value of 0.18 indicating a mismatch of roughly 18%.

In a first attempt to fit the model output to measurement data six response traces were selected, at beam positions 2.5, 3 and 3.5, each in both the *x* and *z* direction of the axis system. Using initial estimates for the model parameters the sensitivity of the fitness function to a change in each of these parameters was investigated. The average change in the fitness function value to a change in parameter value by an order of magnitude in either direction was required to be at least $1 \cdot 10^{-4}$. This requirement was not met by two parameters, namely the damping values at both extreme ends of the specified frequency range (75 and 3000 Hz). The remaining 20 parameters were included in a genetic algorithm fit in the frequency range 0-500 Hz with a population size of 1000 and 40% elitism (400 individuals). On an average PC (a 3 GHz dual-core machine with 3GB internal memory) this calculation ran for approximately 48 hours before finishing at generation 57. A comparison between measured and fitted spectra showed some discrepancies, especially where the responses in the *x*-direction and at higher frequencies (> 350 Hz) were concerned. This may be because the excitation may not have been purely in the *z*-direction, because no direct coupling between the bending modes in both orthogonal directions has been included in the model or (in the case of the high-frequency modes) because the element size is too coarse for an accurate description.

Given the above result and the fact that most features which are indicative of damage are expected to be observable in the response curve in the *z*-direction at lower frequencies ($\leq$ 350 Hz) a second global fit was made using only the mobilities in the *z*-direction and a frequency range of 0-350 Hz. All 22 parameters were included in the fit, which again had a population size of 1000 with 40% elitism, ran for another 48 hours and finished at generation 58. This fit converged to roughly the same corner of parameter space as the previous one, indicating that

the global optimum had indeed been reached. In a third and last optimization step a local optimizer including all 22 parameters was run on the obtained solution to give the global minimum. The result, with a fitness function value of 0.2780, is displayed in Figures 6 through 8. As can be seen the correspondence is rather good, especially given the fact that the absolute response in Figure 7 is over 2 orders of magnitude smaller than at the other two positions and measurement noise may therefore be relevant here.

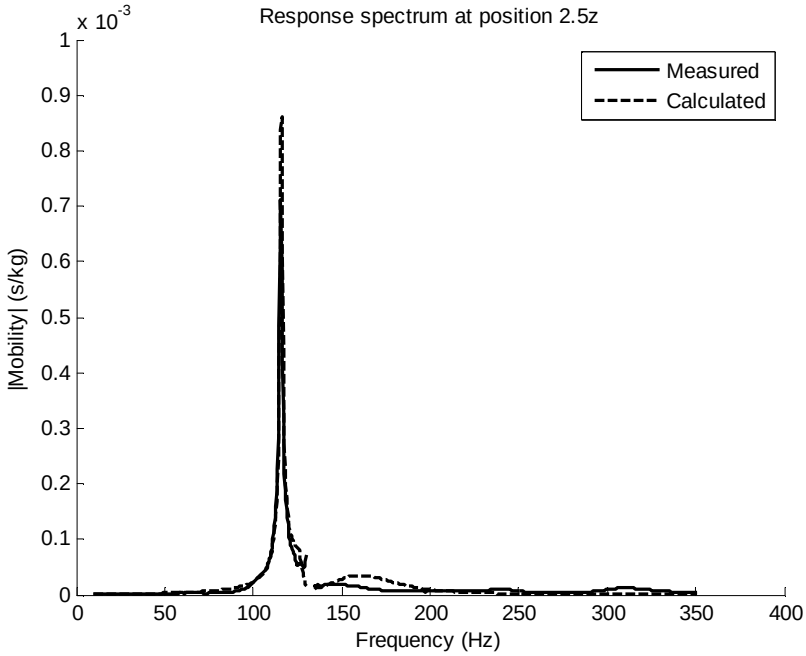

Figure 6: Measured and calculated mobilities in the *z*-direction in the middle between support bars 2 and 3 for an excitation force in *z*-direction between support bars 3 and 4

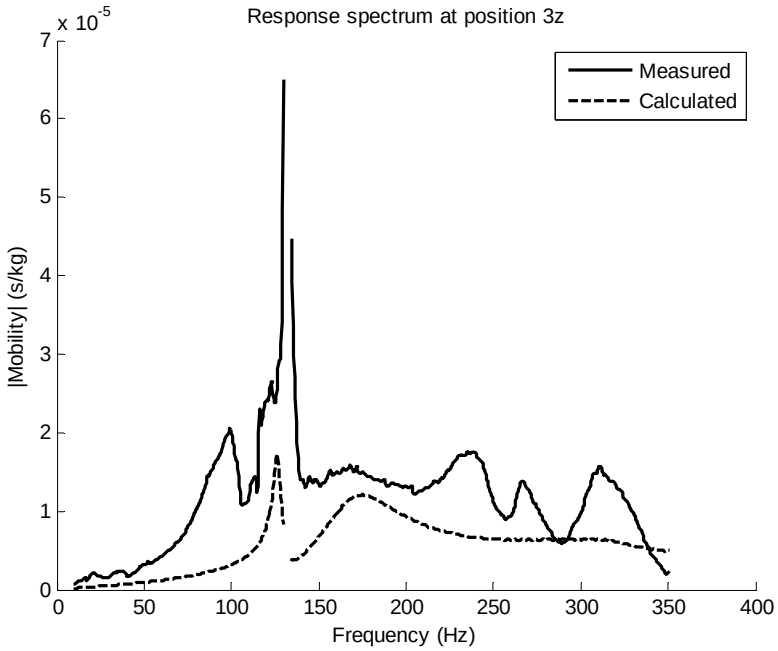

Figure 7: Measured and calculated mobilities in the *z*-direction above support bar 3 for an excitation force in *z*-direction between support bars 3 and 4

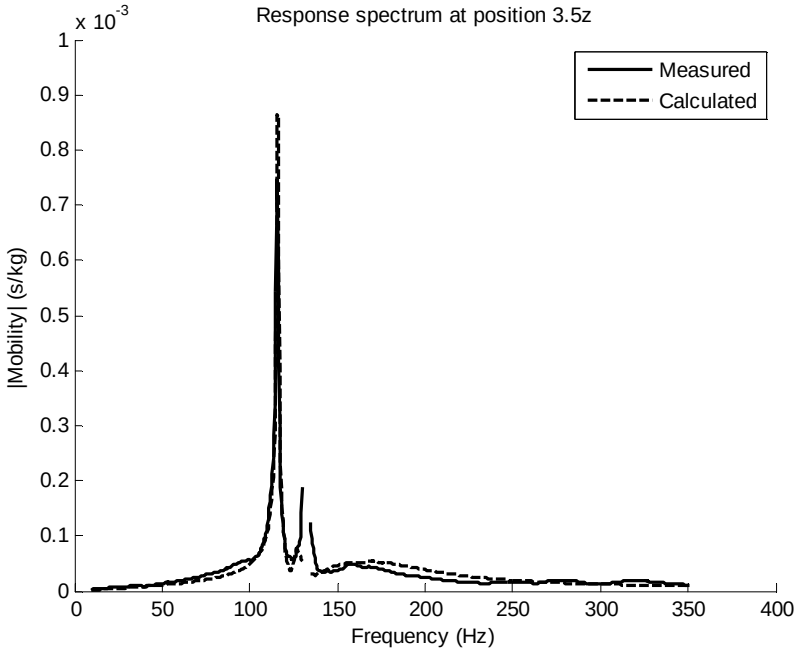

Figure 8: Measured and calculated mobilities in the *z*-direction in de middle between support bars 3 and 4 for an excitation force in the same direction and position

4.3 Damage detection

As mentioned in section 2.1 in the current measurement setup the total number of parameters in the model is much larger than the number of available measurement traces. Given the possibe non-uniqueness of a solution to the inverse problem it is unwise to try and unambiguously fit all parameters to the available data. The effects of the types of damage, to be considered by the model, on the model parameters should therefore be estimated before a fit is attempted. Here the same damages as investigated in the lab test (section 3.2) were included.

Control spring failure

This type of damage was modeled as zero support bar spring stiffness in the *x*-direction, the effect of which was not visible on any of the spectra observed here. This type of damage will therefore not be discussed further.

Support failure

In the lab tests the effects of sliding supports breaking off was investigated by removing a single sliding support of the third support bar, on the side furthest away from the beam, as well as by removing both sliding supports for the same support bar in a second test. This was modeled by setting all support bar spring stiffnesses for the respective sliding support(s) equal to zero. For the missing support on a single side it was also found that the best agreement between model and experiment could be found if the modal damping factor at 75 Hz was reduced from 15 % to 9 % while the damping factor at 118 Hz was increased from 0.3164 % to 0.65 %. The spectrum at position 3 for this one-sided damage case is given in Figure 9.

From this spectrum it can be deduced that a new mode has appeared at around 26 Hz which is especially strong over the support bar. Although the frequency of this mode is slightly overpredicted by the model (28 Hz) the agreement in position and relative mode intensities is very good. Even more subtle effects are reproduced very well: at all frequencies apart from the new mode the response is observed to be slightly higher at position 2.5, slightly

lower at position 3.5 and significantly lower at position 3, and the peak at around 118 Hz which for the undamaged case is present at position 3 has disappeared for the damaged case, all in accordance with model predictions. A decreased response in the main mode at 118 Hz in the spectra at positions 2.5 and 3.5 is fitted by the aforementioned increased modal damping factor at this frequency. It can therefore be concluded that this type of damage is clearly visible in the spectra presented here and identification of this damage mode should therefore be possible.

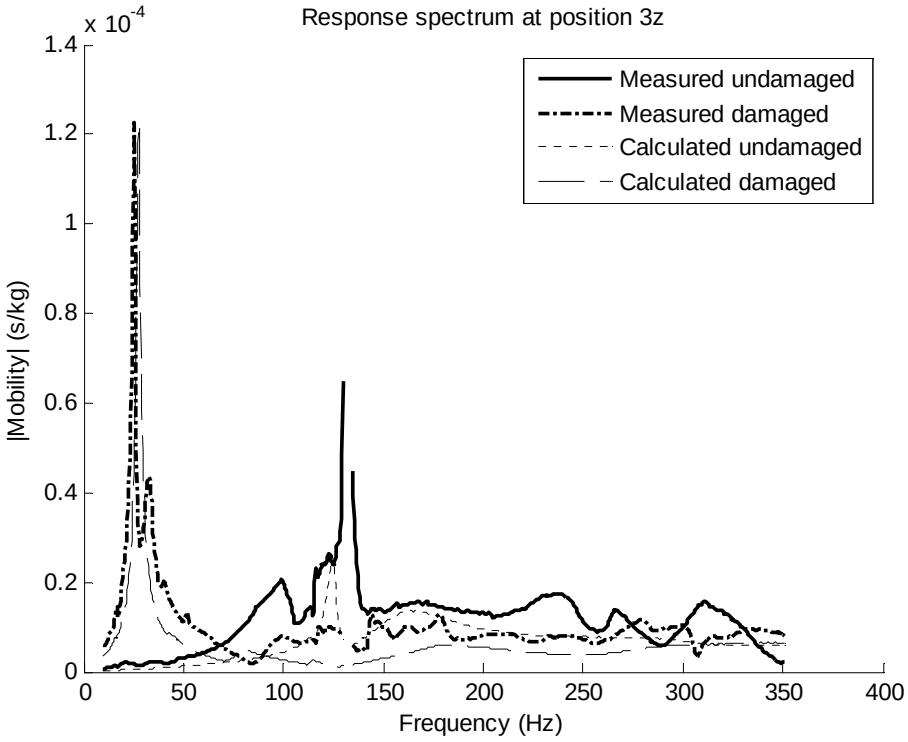

Figure 9: Effect of a single sliding support breaking off on the mobility spectrum at position 3

Half saw cut in a support bar

In the lab experiments this type of damage to a support bar was tested by making a cut in the vertical direction (the long axis of its cross section) over the full width of the support bar. In this configuration the cross sectional area, shear cross sectional area, bending inertia about the *z*-axis and torsional inertia about the *x*-axis all decrease linearly with increasing depth of the cut while the bending inertia about the *y*-axis decreases with the third power of this depth. For a different type of cut or different geometries like that of the beam, however, these dependencies could be different. Nevertheless, the same dependency was assumed for the beam as well (with *x*- and *y*-axes interchanged following its different orientation).

The effect the cut in support bar number 3 has on the measured mobilities is displayed in Figure 10. The only effect that can be observed at positions 2.5 and 3.5 is an increased damping in the main mode at 118 Hz. It was found that the measured spectra could best be reproduced using a modal damping value of 0.7% at this frequency. At position 3 the response at all frequencies up to about 250 Hz is significantly higher for the damaged case, most notably in the 118 Hz-mode. All these effects are accurately predicted by the model used here. Nevertheless, the absolute changes in the measured responses are relatively small, especially when considering the fact that a 50% cut was used for this experiment. Normally, actual cracks will of course be much smaller and their effects therefore even less visible than observed here.

Additionally, comparing the observed changes to the mobility spectra with other damage mechanisms considered in the current investigation, the question of uniqueness of the effects of this type of damage to a support bar arises once again. In a real life situation it is therefore unlikely that the existence of a crack in a support bar can be deduced from the mobilities observed here.

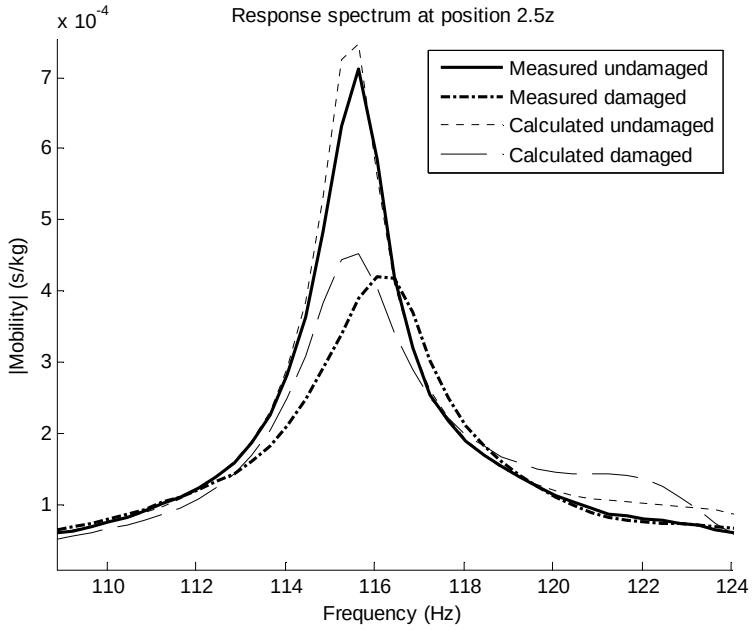

Figure 10: Effect of a 50% cut in support bar 3 on the mobility spectrum at position 2.5

Half saw cut in center beam

From the measured spectra (see Figures 11 and 12) it can be decuded that, most interestingly, the frequency of the main mode at positions 2.5 and 3.5 has descreased by 6 Hz and the intensity has decreased considerably as well. These effects are reproduced very well by the model, although the actual intensity of the responses for positions 2.5 and 3.5 is somewhat underestimated. Around the same frequency the peak in the mobility spectrum at position 3 seems to have split up into two separate peaks, one at a slightly lower and another at a slightly higher frequency. Whereas this splitup and the resulting frequencies are again reproduced by the model the intensity of the lower frequency mode (corresponding with the main peak at positions 2.5 and 3.5) is severely underestimated. It can be concluded nevertheless that the effect of a 50% cut in the beam can be observed very well and can clearly be distinguished from the effects of other types of damage. However, as with the crack in a support bar discussed above, it is questionable whether a clear reponse will be visible for a more real-life situation where the expected crack depth is small.

Loose joint

A weld failure between beam and support bar was reproduced in the model by setting all moments of inertia for the connection element to zero. Simultaneously the cross sectional area and shear cross sectional area for this element should be lowered. The actual value to be used is hard to predict since it is an effective value: upward motion of the beam is unhindered in case the connection between beam and support bar has failed, corresponding with zero area for the connection element. Downward motion of the beam, however, is unaltered since the support bar itself is still present. The reduction factor to be used for the cross sectional area and shear cross sectional area was therefore deduced from a comparison between the model

and experiment. A value of 1e-3 was found to give the best correspondence. Lastly, the modal damping factor for the main mode at 118 Hz was increased to 0.5%. The resulting model calculations and a comparison with experiment are given in Figure 13.

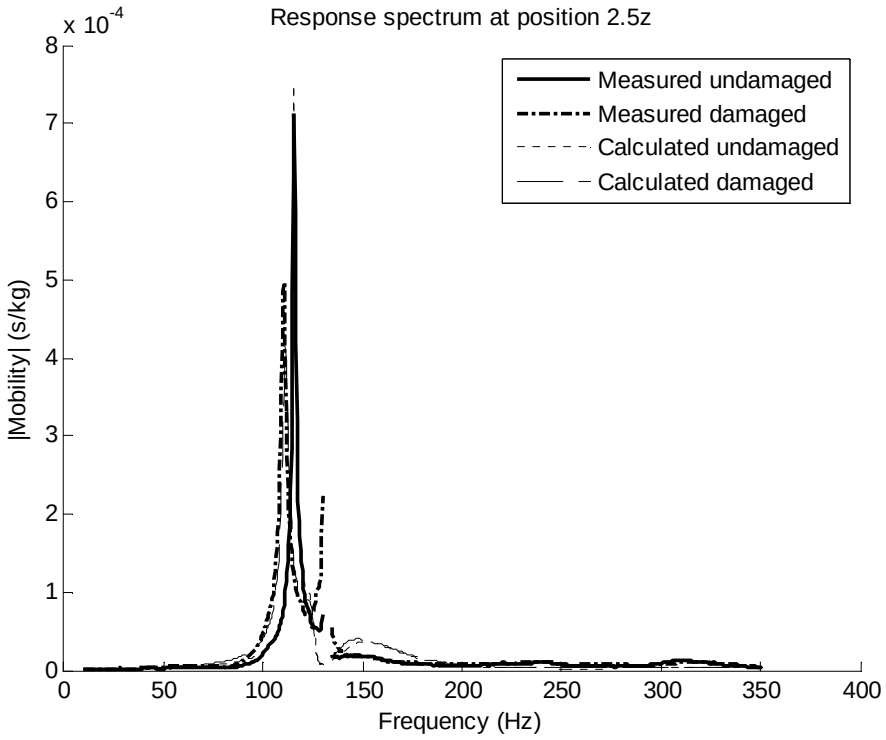

Figure 11: Effect of a 50% cut in the beam on the mobility spectrum at position 2.5

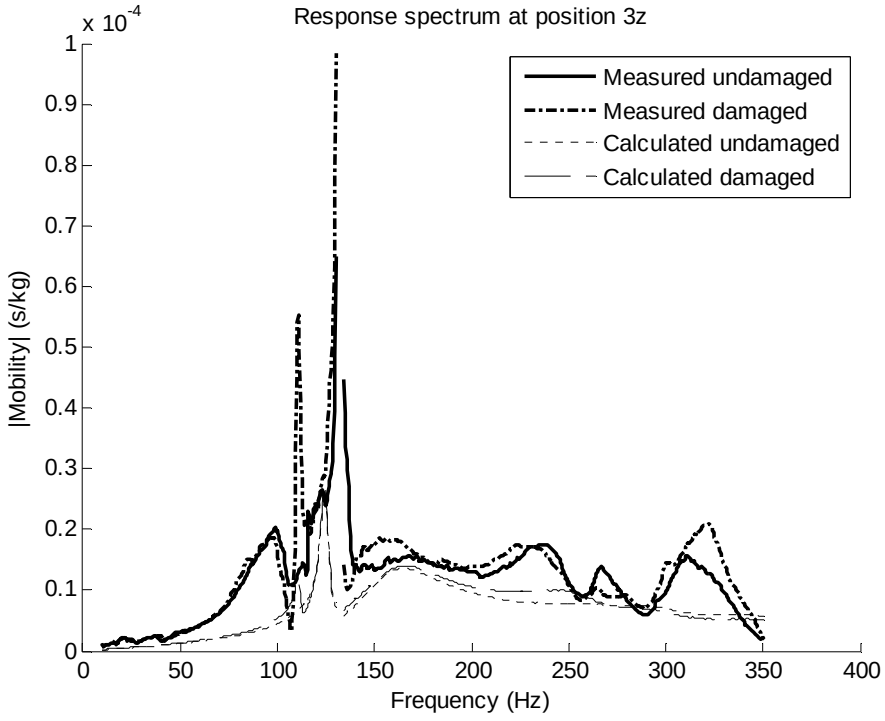

Figure 12: Effect of a 50% cut in the beam on the mobility spectrum at position 3

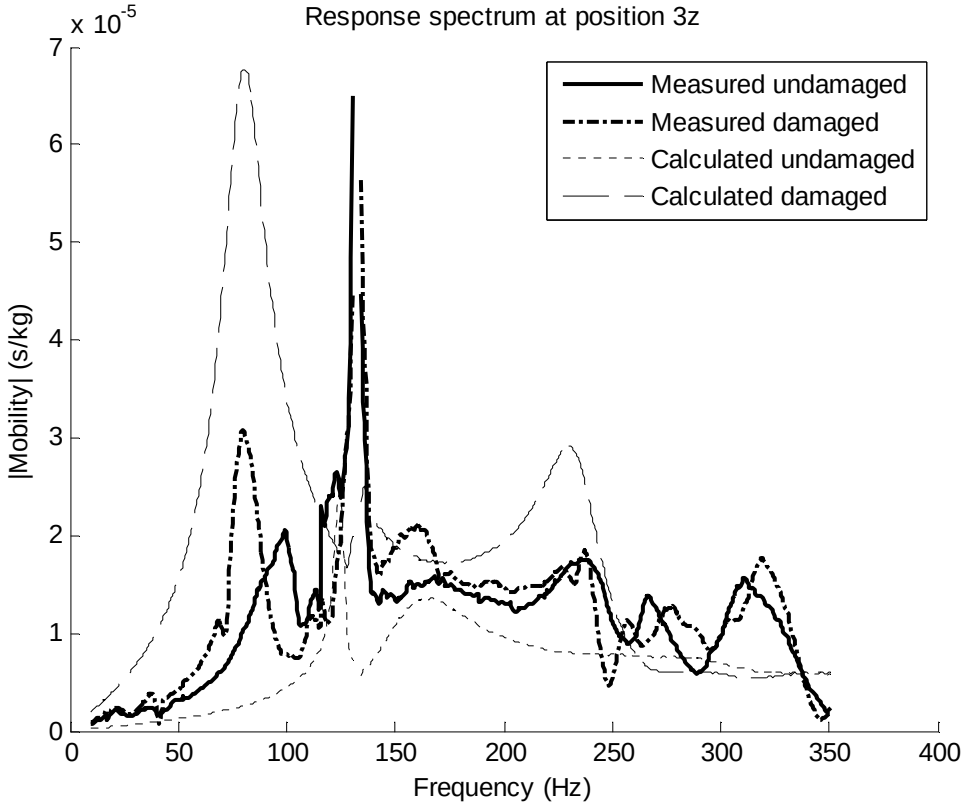

Figure 13: Effect of failure of a weld between beam and support bar at position 3 on the mobility spectrum at this position

Not surprisingly the largest effect for this type of damage can be observed above the support bar, where a very strong mode has appeared at a frequency of 79 Hz. The same mode is also present in the other two spectra, although much more weakly. Furthermore the intensity distributions are changed in all spectra, most notably above the support bar where it is much stronger in the range 0-250 Hz than for the undamaged case. All these effects, including even the minor changes in relative mode intensities at positions 2.5 and 3.5, are predicted perfectly by the model. The only blemish is the fact that in the damaged case the intensity for the new mode at 79 Hz is overestimated, in contrast with the underestimated response for the undamaged case. The predicted effects can also clearly be distinguished from those of other damages. Combined with the fact that weld failure is a binary effect which will always lead to the same amount of damage it can be safely concluded that this type of damage can easily be detected and identified. However, the fact that the cross sectional area and shear cross sectional area had to be fitted to the experimental data rather than determined from first principles is somewhat disappointing. It might be that the value of 1e-3 used here is different for other joint geometries or even other types of excititation and should therefore be redetermined for every analysis.

Combined damages

With respect to combined damages the inverse modeling confirms the conclusions obtained from the experiments: the effects of combined damages can well be approximated by adding the effects of each separate type of damage.

5 DEGRADATION MODEL

5.1 Defect initiation and growth

The process of degradation can often be well described as random due to poor inspection, lack of data or other sources of uncertainty. Stochastic processes have been widely used in order to investigate inspection strategies under stochastic degradation (see for example [3] and [4]). When the degradation process is to be modeled by continuous quantities in time, for example wall thickness loss or corrosion growth in time, then the gamma process is more natural [5]. When the degradation process is modeled by changes of one state to another in time then Markov chains are more suitable [6]. According to [5] the gamma process has been successfully fitted to data on creep of concrete, fatigue crack growth, corroded steel gates, thinning due to corrosion and chloride ingress into concrete. On the basis of the gamma deterioration process, case studies have been performed to determine optimal dike heightening, optimal sand nourishment sizes, optimal decisions for steel coatings and optimal inspection intervals for high speed railway tracks, berm breakwaters, steel pressure vessels, automobile brake pads, and block mats and rock dumping of the Eastern-Scheldt barrier in the Netherlands. In this paper a tool that investigates deterioration through the gamma process is introduced. The model is taken from [7]. The Poisson process is used to model initiation times while the gamma process is used to model deterioration growth.

The Poisson process is a counting process. This is a random function N: $\mathbb{R}^+ \rightarrow \mathbb{R}$ such that:

- $N(0) = 0$ and $N(t) \in \{0, 1, 2, 3, \ldots\}$ for all t
- if $s < t$ then $N(s) < N(t)$

Following [8] the homogeneous Poisson process will be defined by equation (2). $N(a_i, b_i]$ denotes the number of events (degradation initiation in our case) falling in the half-open interval $(a_i, b_i]$ with $a_i < b_i \leq a_{i+1}$.

$$P\{N(a_i,b_i) = n_i,\ i = 1,\ldots,k\} = \prod_{i=1}^{k} \frac{[\lambda(b_i - a_i)]^{n_i}}{n_i} e^{-\lambda(b_i - a_i)} \tag{2}$$

The parameter λ can be interpreted as the mean rate of occurrence or intensity. The non-homogeneous Poisson process with time dependent rate λ(t) can be defined exactly as in equation (2) with the quantities $\lambda(b_i - a_i) = \int_{a_i}^{b_i} \lambda dx$ replaced whenever they occur by quantities:

$$\Lambda(a_i,b_i) = \lambda \int_{a_i}^{b_i} m(x)dx \tag{3}$$

In this case, the parameter λ will be referred to as the proportionality constant. In a general framework this parameter may be used in a Bayesian analysis. It will be considered uncertain and in order to update the model we could use the number of defect observed in a given time interval.

In a gamma process a random variable X has a gamma distribution with shape parameter $v>0$ and scale parameter $u>0$ if its probability density function is given by:

$$ga(x \mid v(t),u) = \frac{u^{v(t)}}{\Gamma(v(t))} x^{v(t)-1} e^{-ux} I_{(0,\infty)}(x) \tag{4}$$

where $I_A(x) = 1$ for $x \in A$ and $I_A(x) = 0$ for $x \notin A$, and $\Gamma(a) = \int_{z=0}^{\infty} z^{a-1} e^{-z} dz$ is the gamma function for $a>0$. If $v(t)$ now is a non-decreasing, right continuous, real valued function for

$t \geq 0$ with $v(0) \equiv 0$ then the gamma process with shape function $v(t)>0$ and scale parameter $u>0$ is a continuous-time stochastic process $\{X(t);\ t \geq 0\}$ such that:

- $X(0) = 0$ with probability one
- $X(s) - X(t) \sim ga(\cdot|v(s) - v(t); u)$ for all $s > t \geq 0$
- X(t) has independent increments

From this definition the first hitting time distribution can be derived, which is the distribution of the first time at which the defect size is larger than a given defect size y. It is denoted by T_y and it is given by

$$F_{T_y}(t) = P(T_y \leq t) = P(X(t) \geq y) = \int_y^{\infty} ga(x, v(t), u)dx \tag{5}$$

5.2 Deterioration process

The deterioration process will be defined following [7] as a combination of defect initiation and defect growth. Defects will initiate according to a Poisson process (homogeneous or not) and will grow independently according to the gamma process. The probability density function (pdf) of the k^{th} arrival time ($S_k : 1 \leq k \leq n$) conditional on n defect initiations up to time t (for fixed t) is given by

$$f_{S_k|N(t)} = n(s) = \frac{n!}{(k-1)!(n-k)!}\left(\frac{\Lambda(s)}{\Lambda(t)}\right)^{k-1}\left(1-\frac{\Lambda(s)}{\Lambda(t)}\right)^{n-k}\frac{\lambda(s)}{\Lambda(t)} \tag{6}$$

The depth D_k of the k^{th} defect at time t will be defined as the growth according to a gamma process in the time interval between its initiation and t, that is, $D_k = X(t-S_k)$. Assuming that the process $X(\cdot)$ is independent of the arrival times S_k and using equation (6) we obtain:

$$P(D_k \leq x \mid N(t) = n) = \int_0^t P(X(t-s) \leq x) f_{S_k|N(t)=n}(s)ds \tag{7}$$

Under our assumption that we have knowledge that n defects have initiated up to time t we could ask what the distribution is of the size of a randomly selected defect at time t. This is given in the equation below.

$$P(D_k \leq x \mid N(t) = n) = \int_0^t P(X(t-s) \leq x)\frac{\lambda(s)}{\Lambda(t)}ds \tag{8}$$

5.3 Failure probability

We assume that our component fails as soon as a defect is deeper than a certain defect size y. Let $N_x(t)$ denote the number of defects deeper than x for $x > 0$ up to time t. Then the probability that no system failure occurs up to t is given by $P(N_y(t) = 0)$. It may be shown that the process $N_x(t)$ is also a Poisson process with intensity given by

$$\Lambda_x(t) = \lambda\int_0^t F_{T_x}(t-s)m(s)ds \tag{9}$$

We define the event $A_x(t)$ as the event of observing at least one defect larger than x within the time interval $(0, t]$. Since the event $N_x(t)$ is also a Poisson process then

$$P(A_x(t)) = 1 - e^{\Lambda_x(t)} \tag{10}$$

5.4 Structural assessment

The idea behind full-scale measurements is that ambient vibrations measured by e.g. strain meters are used as input for the damage detection model described in section 4. This will result in information regarding the number of defects present in the joint, the types of defects and the extent of each. These data could then be used to continuously update estimates of the degradation model parameters described above: the proportionality constant λ describing the rate of occurrence of defect initiation and the shape parameter v and scale parameter u describing the progression of defects after initiation. In absence of sufficient data to deteremine reliable values for the latter two parameters they can be estimated by structural experts from typical times after which certain levels of degradation are expected to be reached. With increasing measurement time the defect parameter estimates will become more accurate, enabling the asset manager to reliably determine when specified minimum performance criteria will be reached and maintenance should be planned.

6 SETTING UP AN EXPERIMENT

In the previous sections all aspects of damage detection using inverse analysis have been discussed in theory and checked against lab experiments on a bridge joint. It was found that under these controlled conditions at least some types of damage can indeed be detected and the corresponding damage parameters derived. This result shows that the more general approach to inverse analysis also applies to a bridge joint. The success or failure of a certain type of experiment can often be reliably predicted before the actual experiment is even performed.

When setting up an experiment for an inverse problem one should in general follow the procedure outlined in Figure 14, which starts with a definition of the parameters that are to be determined in the analysis (for the case discussed in this paper the different types of damage which are to be distinguished). A model of the problem can then be set up and its response to different types of input (for example the different damage types) analyzed. This will provide the user with information about the number of detectors that has to be used as well as their optimal placement in order to avoid ill-conditioning. The amount of detail used at this stage is of critical importance. This is also the point where, in the case of environmental vibration monitoring, the question should be answered which (prefarably force-independent) parameters should be monitored (for example mobilities). Lastly, the effect of the excitation location(s) and possible locations of damage should be considered, since for many types of damage changes in observables are mainly visible near these locations.

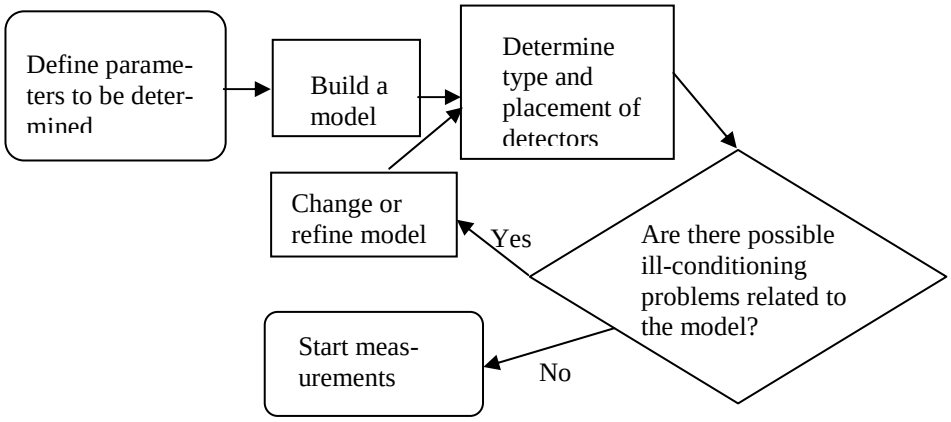

Figure 14: Procedure for setting up an inverse detection experiment

Using the information obtained above the user should be able to assess from calculated sensitivities whether any ill-conditioning is to be expected and whether all parameters of interest can be uniquely determined. If not the user can attempt to change or refine the model based on these observations in order to remedy the situation. Only when all issues have been solved can the experiment be started. If a problem persists despite changes to the model and/or detector placement it has to be concluded that it is not possible to reliably detect the parameters the user is interested in with the type of experiment under consideration.

After an experiment has been conducted the system response as predicted by the model needs to be fit to the actual response by variation of model parameters which are not well known (tuning of the model). In the current investigation it was found that in practical situations a model response (such as for the FEM model used here) quickly becomes so complex that a local optimization routine can no longer be used. A genetic algorithm was therefore chosen, which performed very well. As a good alternative neural networks could also be considered but their use was not explored here. The genetic algorithm might also be used to determine the optimal detector placement as part of the setup of an experiment as outlined in the previous paragraph.

In the case of continuous measurements the response of the tuned model can be compared with the measurement data at every timestep. When the discrepancy is greater than a predetermined threshold it is concluded that damage has occured and a refit of the model will be requested to determine the type of damage and the corresponding damage parameters. Since the model will usually contain far too many parameters to be able to determine all of them possible damages will have to be explicitly specified and included in the model refit as possible causes for the observed change in system response. This does mean that the damage detection system will only be able to identify those damages which have been considered at the outset of the experiment.

For the types of damage which occur gradually it is also important to determine at which point damage becomes visible as a change in variables. The answer to this question obviously depends on many different factors such as the level of detail of the model used in the analysis and the measurement noise. The threshold on the fitness function used to identify damages should be set accordingly. If, for example, a change in the fitness function value of 0.01 is taken as an indication of damage and the cause of this change is a crack in a beam, then for the model considered here a crack with a minimum depth of 1.5% of the beam height, corresponding with 1.8 mm, should be observable. Depending on the cause for the formation of this crack this may or may not coincide with the moment of crack appearance.

7 FULL-SCALE TESTS

In order to test the models described above full-scale measurements are performed on a bridge in the Netherlands. From mid to end June 2010 a monitoring system was installed in order to measure strain deformation in steel parts. However, given the recent installation of these strain gauges as compared to the bridge design lifetime insufficient information has yet been obtained to derive the necessary defect parameters. Detailed results of this ongoing effort will be presented in future publications.

8 CONCLUSIONS

In this paper lab measurements of the dynamic response of a damaged bridge expansion joint were discussed. It was found that several of the more common types of damage could reliably be discriminated and quantified through the use of genetic algorithms for the determination of key parameters in a FEM model. Given these promising results full-scale tests were

started on an actual bridge expansion joint installed in a highway bridge in the Netherlands. Since no results from the full-scale tests are available yet thought should be given to the question as to how far the results obtained for the lab model can be extended to a full-size bridge joint. The number of model parameters for a full-sized joint is obviously larger than that for the lab model, but this is offset by the fact that the overall geometry of a joint is very regular. This means that, although larger, the model for the full-sized joint will most likely not be any more complex. The same types of spectra and effects can therefore be expected. Moreover, since lateral movement of the actual joint will be much more constricted than was the case for the lab model, unlike the lab model case it might even be possible to use the mobility spectra in this direction in the fitting procedures, which might help to alleviate some of the ill-posedness which was observed in the lab tests.

The quality of data from the actual bridge joint depends on many factors such as the number, type and sensitivity of the detectors used in the experiment, their placement and the amount of traffic across the bridge. However, given suitably large averaging times there is principally no reason to assume that data obtained for the full-sized joint should be of lower quality than those obtained from the lab tests. Since in the lab tests mobilities were observed, which are independent of the excitation force, the use of ambient vibrations as an excitation source should also not affect the suitability of the method investigated here. In conclusion, damage detection by environmental vibration monitoring is a feasible method for use with a bridge expansion joint.

REFERENCES

[1] H. Wenzel, D. Pichler, *Ambient Vibration Monitoring*, Wiley, 2005.

[2] G.R. Liu, X. Han, *Computational Inverse Techniques in Nondestructive Evaluation*, CRC Press, 2003.

[3] J.M. van Nortwijk, *Optimal Maintenance Decisions for Hydraulic Structures under Isotropic Deterioration*, Phd thesis, TU Delft, 1996.

[4] M.J. Kallen, *Markov Processes for Maintenance Optimization of Civil Infrastructure in the Netherlands*, Phd thesis, TU Delft, 2007.

[5] J.M. van Noortwijk. *A Survey of the Application of Gamma Processes in Maintenance*, Reliability Engineering & System Safety, 94(1):2 – 21, 2009.

[6] M.J. Kallen, *A Comparison of Statistical Models for Visual Inspection Data*, Proceedings of the Tenth International Conference on Structural Safety and Reliability (ICOSSAR), pages 3235 – 3242, Osaka, Japan, 2010.

[7] S.P. Kuniewski, J.A.M. van der Weide, J.M. van Noortwijk, *Sampling Inspection for the Evaluation of Time-dependent Reliability of Deteriorating Systems under Imperfect Defect Detection*, Reliability Engineering & System Safety, 94(9):1480 – 1490, 2009.

[8] D.J. Daley, D. Vere-Jones, *An Introduction to the Theory of Point Processes, Volume 1*, Springer, 2nd edition, 2002.